analytical chemistry

Article

pubs.acs.org/ac

Single-Cell Lipidomics: Characterizing and Imaging Lipids on the Surface of Individual *Aplysia californica* Neurons with Cluster Secondary Ion Mass Spectrometry

Melissa K. Passarelli,*[,†,‡] Andrew G. Ewing,[‡,§] and Nicholas Winograd*[,†]

[†]Department of Chemistry, The Pennsylvania State University, University Park, Pennsylvania 16802, United States

[‡]Department of Chemistry and Molecular Biology, The University of Gothenburg, SE-41296 Göteborg, Sweden

[§]Department of Chemical and Biological Engineering, Chalmers University of Technology, S-41296 Göteborg, Sweden

Supporting Information

ABSTRACT: Neurons isolated from *Aplysia californica*, an organism with a well-defined neural network, were imaged with secondary ion mass spectrometry, C_{60}-SIMS. A major lipid component of the neuronal membrane was identified as 1-hexadecyl-2-octadecenoyl-*sn*-glycero-3-phosphocholine [PC(16:0e/18:1)] using tandem mass spectrometry (MS/MS). The assignment was made directly off the sample surface using a C_{60}-QSTAR instrument, a prototype instrument that combines an ion source with a commercial electrospray ionization matrix-assisted laser desorption ionization (ESI-MALDI) mass spectrometer. Normal phase liquid chromatography mass spectrometry (NP-LC–MS) was used to confirm the assignment. Cholesterol and vitamin E were also identified with in situ tandem MS analyses that were compared to reference spectra obtained from purified compounds. In order to improve sensitivity on the single-cell level, the tandem MS spectrum of vitamin E reference material was used to extract and compile all the vitamin E related peaks from the cell image. The mass spectrometry images reveal heterogeneous distributions of intact lipid species, PC(16:0e/18:1), vitamin E, and cholesterol on the surface of a single neuron. The ability to detect these molecules and determine their relative distribution on the single-cell level shows that the C_{60}-QSTAR is a potential platform for studying important biochemical processes, such as neuron degeneration.

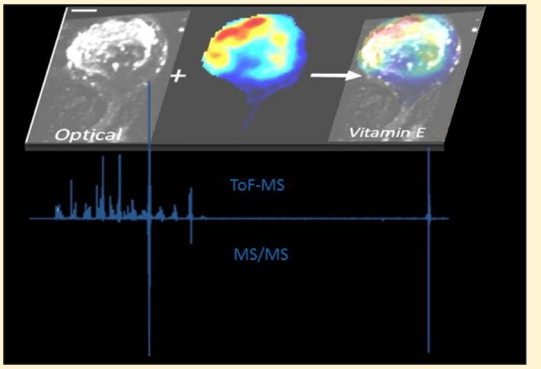

Imaging mass spectrometry (IMS) is emerging as a powerful tool in biochemistry for its ability to simultaneously acquire chemical and spatial information directly off the surface of biological materials. Currently, secondary ion mass spectrometry (SIMS), matrix-assisted laser desorption ionization (MALDI), and desorption electrospray ionization (DESI) are the three main techniques in this methodology.[1,2] For tissue-imaging acquisitions, the three techniques provide a complementary perspective;[3] however, for imaging on the cellular and subcellular level, SIMS is currently the only viable IMS technique.[4−6] Although MALDI and DESI have demonstrated sensitivity sufficient for single-cell detection,[7,8] technical constraints associated with their probe size prevent the techniques from achieving lateral resolutions below 10 and 200 μm, respectively.[9] SIMS is set apart from these techniques due to its ability to achieve submicrometer lateral resolution.

Two regimes exist within the field of SIMS, static and dynamic. In the dynamic regime, known as nanoSIMS, sub-50 nm spatial resolution is obtained for atomic and diatomic species. In order to visualize the distribution of lipids or biomolecules within a single cell, a method known as multi-isotope imaging mass spectrometry (MIMS) is used.[10] In the static regime, the softer ionization dynamics characteristic of cluster ion sources allow for the detection of intact lipid species or metabolites; however, the spatial resolution is typically between 100 nm and 1 μm.[11,12]

Conventional lipidomics investigations are performed using an ensemble of cells, which provides insight on the average chemical composition of the cells. Unfortunately, in this process, the unique characteristics of individual cells are lost and the ability to link the unique chemical composition of individual cells to their respective biochemical functions is convoluted. The unique feature of this cell would be lost with conventional lipidomic investigations. Fortunately, with SIMS not only can the lipid composition be characterized on a single-cell level, but the relative spatial distribution of these lipids can also be obtained. Here, we focus on the R2 neuron of *Aplysia* as it is unique and can be easily identified. This cell is typically the largest cell in the right hemisphere of the abdominal ganglia.[13] The early appearance of this cell during development and its conservation across evolutionarily related species hints to the significance of this one unique cell.[14,15]

Received: October 18, 2012
Accepted: January 16, 2013

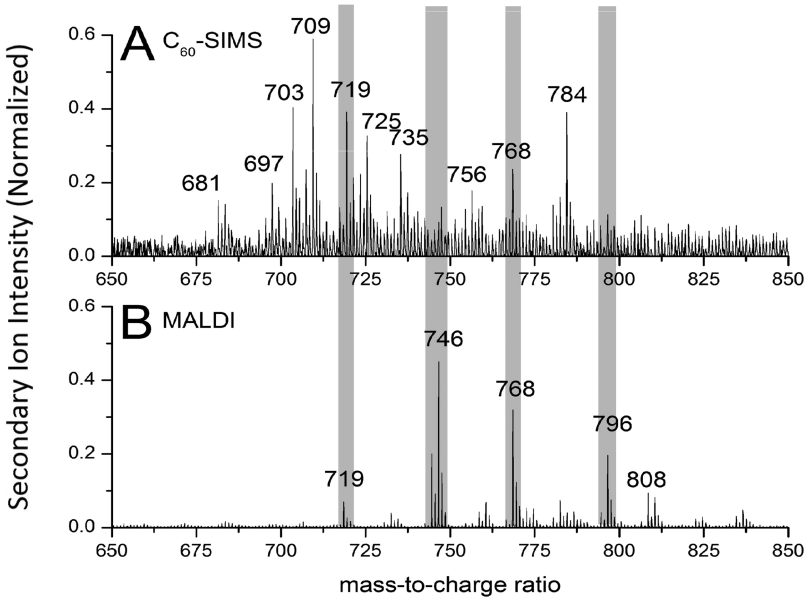

Figure 1. Lipid profiles, mass range m/z 650−850, obtained from the surface of a single *Aplysia* neuron using C_{60}-SIMS (A) and MALDI (B). The MALDI spectrum was normalized to the integrate counts of the maximum peak at m/z 746.5, and the SIMS spectrum was normalized to the integrate counts of the maximum peak at m/z 709.5.

The neural network of the *Aplysia californica* is a well-studied model system for complex neurological processes, particularly learning and memory storage.[14,16] There have been a number of electrochemical,[17−19] electrophysiological,[20,21] and mass spectrometry[22−26] investigations focused on characterizing the *Aplysia* neurons. Despite the range of analyses previously performed, only a limited number of investigations focused on characterizing the lipid distribution of this model system.[27,28] The relatively large size of the neurons in the *Aplysia*'s neurological system allows the dissection and extraction of individual cells by hand with the assistance of a light microscope.[16] Its simplicity allows the characterization of the *Aplysia*'s nervous system, by examining the morphology, intraneural associations, and stimulated response of individual neurons.[13]

In this study, we examine individual neurons from *A. californica*. Localization of various intact lipid species across the surface of a single neuron was mapped using C_{60}-SIMS. The molecular-specific secondary ion images of the *Aplysia* R2 neuron reveal the distribution of a variety of lipid species across the surface of the cell. In addition, tandem MS analyses were employed to deconvolute isobaric interferences and help identify the detected lipid species. This method is routinely employed in MALDI and DESI investigations; however, the design of commercial TOF-SIMS instruments is not compatible with tandem MS capabilities. In this method, the unknown lipid molecule is isolated, fragmented in a collision-induced dissociation (CID) cell, and the resulting fragments provide vital structural information that assists in the identification of the lipid molecule. Piehowski et al. have previously used tandem MS to identify m/z 147 as a major cholesterol fragment and used this fragment to map the distribution of cholesterol on the surface of macrophages (J774).[29] In this report, tandem MS spectra are taken in situ and fragmentation pathways were used to identify vitamin E, cholesterol, and the phospholipid species PC(16:0e/18:1). In addition, these spectra were used to extract and compile all molecular specific peaks in order to improve the technique's sensitivity at the single-cell level. Moreover, we present general protocols for the analysis of single-cell samples with SIMS.

EXPERIMENTAL SECTION

Single-Cell Sample Preparation. All chemicals were obtained from Sigma-Aldrich and used without further purification.

To isolate *Aplysia* neurons, routine extraction procedures were used.[28] Briefly, before dissection the *Aplysia* sea slugs were euthanized by injecting approximately 200 mL of 0.35 M $MgCl_2$ solution into their abdominal cavity. The ganglia were extracted and temporarily placed in artificial seawater. To remove the outer sheath the ganglia were then incubated in a protease solution for 10 min. Individual cells were extracted and placed upon silicon substrates.

MALDI Sample Preparation. For MALDI analyses, 2,5-dihydroxybenzoic acid (DHB) was deposited on the surface of the samples using the sublimation method developed by Hankin et al.[30]

Instrumentation. The C_{60}-QSTAR instrument was used to image and analyze the lipid content of the *Aplysia* neuron. The overall design elements of this instrument and its performance, including ion transmission, signal-to-noise, mass resolution, mass accuracy, and tandem mass spectrometry capabilities, have been demonstrated elsewhere.[31] Briefly, the C_{60}-QSTAR instrument combines a 20 keV C_{60}^+ ion source from Ionoptika, Ltd. with a QSTAR XL, a commercial triple-quadrupole orthogonal time-of-flight (TOF) mass spectrometer from Applied Biosystems/MDS Sciex. The prototype instrument has tandem MS capabilities. A differential pumping system is used to sweep secondary ions from the low-vacuum conditions in the sample region into the mass spectrometer without high-voltage extraction methods. The orthogonal orientation decouples the ionization event from the detection scheme and allows for the use of a continuous ion beam without sacrificing mass resolution ($m/\Delta m$ 12 000−15 600). The platform is compatible with a continuous ion beam, which

dx.doi.org/10.1021/ac303038j | *Anal. Chem.* XXXX, XXX, XXX−XXX

Table 1. Dominant Lipid Species Observed in the Spectra in Figure 1[a]

classification [LM_ID]	label (C:DB)	nominal mass	species	SIMS	MALDI
glycerophospholipids/	(PC18:1e/16:0)	709	$[M + Na - N(CH_3)_3]^+$	+++	
glycerophosphocholines/		725	$[M + K - N(CH_3)_3]^+$	++	
1-alkyl, 2-acylglycerophosphocholines		746	$[M + H]^+$		+++
[**GP0102**]		768	$[M + Na]^+$		+++
		784	$[M + K]^+$		++
	PC(18:1e/18:1)	735	$[M + Na - N(CH_3)_3]^+$	++	
		751	$[M + K - N(CH_3)_3]^+$	++	
		772	$[M + H]^+$		++
		794	$[M + Na]^+$		++
		810	$[M + K]^+$		++
glycerophospholipids/	PC(16:0/16:0)	697	$[M + Na - N(CH_3)_3]^+$	++	
glycerophosphocholines/		756	$[M + Na]^+$		++
diacylglycerophosphocholines/	PC(18:1/16:0)	723	$[M + K - N(CH_3)_3]^+$	++	
[**GP0101**]		760	$[M + H]^+$		++
		798	$[M + K]^+$		++

[a]The assignments were confirmed with tandem MS. The relative intensities of each peak for SIMS and MALDI are compared. All peaks were present above the noise level. The symbol ++ denotes that the integrated intensity of the peak is 1−10 times greater than the same peak on the other spectrum, and +++ represents a difference in the integrated peak intensity greater than 10 times that of the same peak on the respective spectrum.

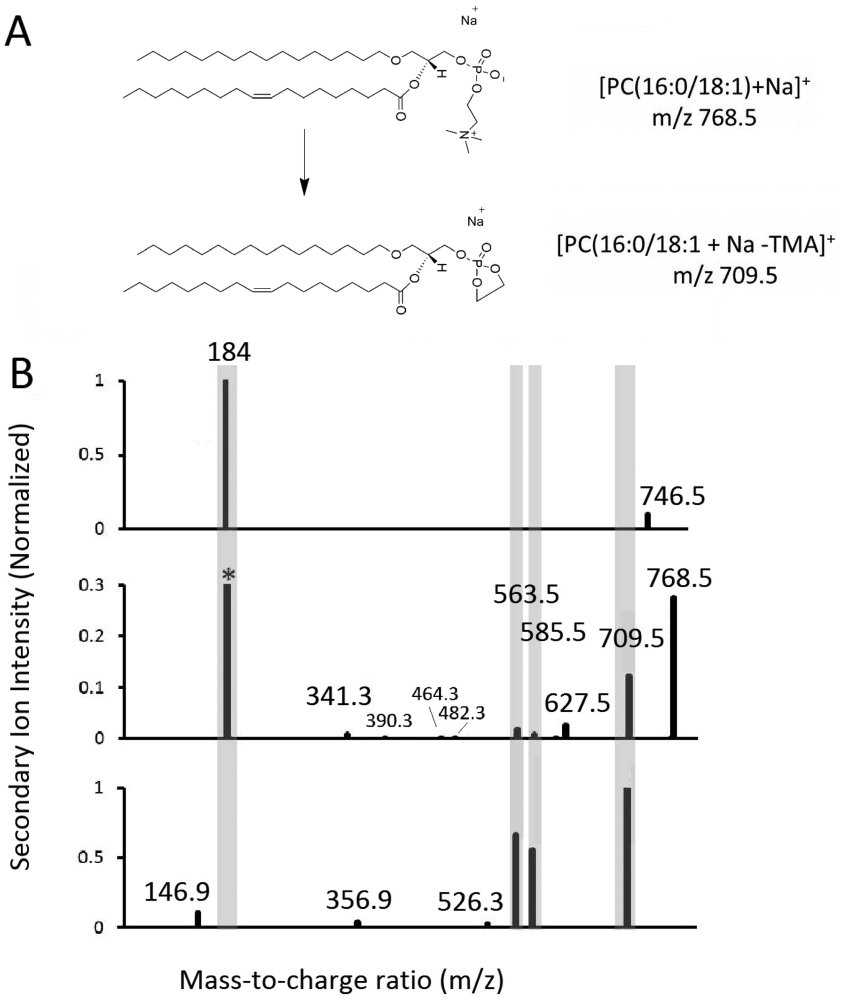

Figure 2. Glycerophosphocholines, e.g., PC(16:0e/18:1), are readily adducted to biological salts (i.e., sodium and potassium). In the gas phase, these lipid-adducted species lose a trimethylamine group from the phosphocholine headgroup to form a high-mass fragment [M + (K or Na) − TMA]. The tandem MS of the protonated lipid species, the sodiated lipid adduct, and the high-mass fragment associated with the loss of TMA are shown, and the common peaks are highlighted. The protonated lipid species provides less structural information than the respective sodiated and high-mass lipid species.

dx.doi.org/10.1021/ac303038j | *Anal. Chem.* XXXX, XXX, XXX−XXX

Table 2. Summary of Fragments Observed in the Tandem MS Spectra in Figure 2B[a]

species	exact mass	formula	MS/MS of $[M + H]^+$	MS/MS of $[M + Na]^+$	MS/MS of $[M + Na - N(CH_3)_3]^+$
$[M + Na]^+$	768.5883	$C_{42}H_{84}NO_7PNa$		768	
$[M + H]^+$	746.6064	$C_{42}H_{85}NO_7P$	746		
$[M + Na - N(CH_3)_3]^+$	709.5148	$C_{39}H_{75}O_7PNa$		709	709
$[M + Na - N(CH_3)_3 - C_2H_5PO_4]^+$	585.5223	$C_{37}H_{70}O_3Na$		585	585
$[M - N(CH_3)_3 - C_2H_5PO_4]^+$	563.5403	$C_{37}H_{71}O_3$		563	563
$[M - R_2]^+$, $R_2 = C_{18}H_{31}O$	482.3611	$C_{24}H_{53}NO_6P$		482	
$[M - R_2 - H_2O]^+$, $R_2 = C_{18}H_{31}O$	464.3505	$C_{24}H_{51}NO_5P$		464	
headgroup fragment	184.0739	$C_5H_{15}NPO_4$	184	184	
headgroup fragment	146.9823	$C_2H_5PO_4Na$		147	

[a]The tandem MS of the protonated lipid species ($[M + H]^+$), the sodiated lipid adduct $[M + Na]^+$, and the high-mass fragment associated with the loss of TMA ($[M + Na - N(CH_3)_3]^+$), where the molecular ion (M) is PC(16:0e/18:1).

allows mass spectra to be collected during the sputtering. The instrument also has a fiber-optic nitrogen laser for MALDI acquisitions.

SIMS images were obtained in positive ion mode. Each pixel was bombarded with a 10 pA C_{60} beam for 1 s. The dimensions for the R2 neuron image were 0.81 mm × 1.91 mm (uncropped, 2 mm × 4.75 mm) at 10 μm step size. The rf transmission in the quadrupole was weighted to improve the transmission of ions in the lipid range: 5% at m/z 50, 25% at m/z 140, and 70% at m/z 370. Tandem MS analyses were performed in situ. In this analysis the precursor ion was selected with unit resolution in the Q_1 mass filter and fragmented using 40 eV of collision energy. For MALDI analyses, the spectral data was summed over 300 laser shots (15 Hz, 20 s) for tandem MS mode acquisitions and 900 laser shots (15 Hz, 60 s) for TOF-MS mode acquisitions.

Data Analysis. To eliminate background signal (i.e., high-mass SiO_2 clusters) from the SIMS images only pixels from the sample region were used for the lipid-based spectral analysis. The mass spectra were binned to 10 bins per dalton. A baseline correction was applied to the SIMS spectrum using MATLAB. Each spectrum was normalized to the intensity of the maximum peak, unless otherwise specified. For imaging, the peak of interest was mapped and the resulting image was smoothed with a cosine filter (three pixel window). The images were normalized first to the total ion image and then to their respective maximum pixel intensity.

To measure the level of commonality between two spectra, the aligned and binned spectra were correlated in MATLAB. In addition, the percentage of peaks the TOF-MS and tandem MS spectra have in common was determined by dividing the total number of common peaks by the total number of peaks in the TOF-MS spectrum (see the Supporting Information).

RESULTS AND DISCUSSION

Single-Cell Lipid Profiles with SIMS and MALDI. Lipid profiles obtained from single cells using C_{60}-SIMS and MALDI after sublimation-based matrix deposition are shown in Figure 1 and summarized in Table 1. The two lipid profiles have very different spectral fingerprints, and each provides a unique perspective to the lipid content of the cell. The major peaks in the SIMS lipid profile were m/z 709.5, 719.5, 725.5, 768.5, and 784.5. Compared to the dominant peaks observed in the MALDI spectrum, at m/z 746.5, 768.5 and 796.5, the SIMS lipid profile is very different from the MALDI lipid profile.

There is an obvious difference in spectral clarity when comparing the lipid region of the MALDI and SIMS spectra (i.e., the MALDI spectrum contains fewer peaks and has less noise compared to the SIMS spectrum). For single-cell imaging experiments, molecular ion sensitivity is often a major challenge due to the limited amount of sample material per pixel area. This leads to the noticeably lower signal-to-noise ratio in the SIMS spectrum compared to the MALDI spectrum. This effect can easily be explained by the different ionization volumes associated with the two techniques. SIMS analysis under static conditions only examines the first few nanometers of the samples surface, whereas the MALDI analysis volume is much larger.[32]

Another obvious difference in the two lipid profiles is observed in the m/z 650−750 mass range. The peaks in this mass range are observed in both spectra; however, these peaks are significantly less dominant in the MALDI spectral fingerprint compared to the SIMS-related lipid profile. These peaks are identified as high-mass lipid-related fragments, produced by the decomposition of sodium and potassium adducted lipids. In this mechanism, the salt-adducted lipid loses the trimethylamine (TMA) moiety in the phosphocholine headgroup, to produce a high-mass fragment with m/z 59 lower than the protonated molecular ion (e.g., [M + (K or Na) − TMA]). This fragmentation pathway, illustrated in Figure 2A, has been previously observed in both electrospray ionization (ESI) and MALDI.[33] In fact, this fragmentation pathway is routinely used with biologically exogenous alkali metal, lithium, to identify phosphocholine.[34] Despite the softer ionization mechanism associated with cluster SIMS, the spectral dominance of these high-mass lipid fragments indicates that the SIMS-based ionization is still harder, more energetic, than MALDI-based ionization.

Lipid Identification. Although IMS-based lipidomic investigations provide valuable spatial information, they prevent exogenous separation techniques that facilitate identification and quantification. Isobaric interference is a major problem with TOF-MS imaging, especially for phospholipid species whose diverse nature but common building blocks produce a variety of ions with similar masses. Lipid assignments are further complicated by biological salts which readily adduct to lipids. Since the proper identification of lipid molecules is crucial in lipidomics-based investigation, tandem MS-related lipid analysis strategies were utilized in this study to help identify various lipid molecules directly from the surface of the sample. While these strategies are routinely employed in MALDI and DESI investigations, in situ tandem MS for lipid identification with SIMS-based analyses is not well-established.

A variety of lipids have the potential to be detected at nominal m/z of 746, the predominant peak in the MALDI spectra. It has been previously tentatively identified as

dx.doi.org/10.1021/ac303038j | Anal. Chem. XXXX, XXX, XXX−XXX

oleoylstearoylphosphatidylethanolamine, PE(18:1/18:0), based on mass accuracy and previous knowledge of the biochemistry.[35] However, the tandem MS spectrum of the unknown lipid at m/z 746 yields only one fragment at m/z 184, which represents the glycerophosphocholine headgroup (see Figure 2A and Table 2). This information assists in discriminating a number of potential lipid species in the identification process but does not provide enough information to make a definitive assignment. As previously reported, with the headgroup information and the nominal mass, the possible assignment can be narrowed to phosphocholine species with 33 carbons and one double bond (PC(33:1)), a phosphocholine species with an ether linkage, 34 carbons, and one double bond (PC(34e:1)), or a phosphocholine species with a plasmalogen linkage, 34 carbons, and no double bonds (PC(34p:0)).[36] A number of lipid molecules with various fatty acid chain lengths are represented by each of these descriptions.

Two of these possible lipid species, PC(34e:1) and PC(34p:0), are ether lipids, a subclass of glycerophospholipids. Although structurally similar to acyl lipids, ether lipids are produced from different starting materials, e.g., fatty alcohols instead of fatty acids, and the biosynthetic pathway is distinct from acyl glycerophospholipids. Structurally, the ether lipids differ from typical glycerophospholipids by the linkage between the glycerol backbone and the fatty hydrocarbon. Plasmalogens are ether lipids with an *O*-alk-1-enyl glycerol fatty alcohol linkage. These two lipids, PC(34e:1) and PC(34p:0), are structural isomers. In order to distinguish them, the location of the double bond needs to be determined. If the double bond is located on the acyl fatty acid moiety then the unknown lipid is PC(34e:1), and if the double bond is located on the ether linked moiety then the lipid is a plasmalogen, PC(34p:0). The tandem MS spectrum of sodiated-adducted lipid revealed which fatty acid tail group contained the double bond.

To obtain more information of the structure of the main *Aplysia* lipid component, tandem MS was performed on the sodiated adduct of m/z 746.5 $[M + Na]^+$, at m/z 768.5 (see Figure 2B). This spectrum reveals fragments at m/z 709.5, 627.5, 585.4, 563.4, 482.3, 464.3, 341.3, and 184.07. The loss of the trimethylamine (TMA) group produces a high-mass fragment at m/z 709, also seen in the TOF-MS spectrum, confirming that the peak is indeed the sodiated adduct of the peak at m/z 746.5. The tandem MS spectrum of the m/z 709 peak is similar to the m/z 746.5 tandem MS spectrum with similar fragment peaks at m/z 585.4 and m/z 563.4. One of the largest differences in these two spectra is the difference in the headgroup-related fragment. The tandem MS spectrum of m/z 709 does not have a peak at m/z 184 ($[C_5H_{15}NPO_4]^+$). Instead the tandem MS of m/z 709.5 has a peak at m/z 147 ($[C_2H_5PO_4Na]^+$), which represents the sodiated adduct of the phosphocholine headgroup with the loss of the trimethylamine (m/z 184 − m/z 59 + m/z 22 = m/z 147).

The lyso-related fragments at m/z 482.3 and 464.3, present in both the tandem MS of peak m/z 746 and m/z 709, can be used to make an unequivocal identification of the unidentified lipid species. These lyso fragments were created by the loss of the fatty acid moiety. In this case, the fatty acid moiety has an m/z value of 281.2, indicative of an 18:1 fatty acid. Upon the basis of this information the lipid is most likely PC(16:0e/18:1). This lipid has an *O*-alkyl ether linkage at the sn-1 position attaching a 16:0 fatty alcohol side chain, a 18:1 fatty acid acyl chain at the sn-2 position, and a phosphocholine group at the sn-3 position of the glycerol moiety.

Overall, the use of tandem MS of protonated molecular ion species in the positive ion mode only reveals information about the subclass of the lipid. Unfortunately, not enough information is provided in this spectrum to make an unequivocal molecular identification. Biological salts are typically a challenge for in situ mass spectrometric investigations due to their detrimental effect on quantification. However, in this investigation, salt−lipid adducts were used to identify the major lipid component in the cell membrane of the R2 neuron of *Aplysia*. The lipid assignment, 1-*O*-hexadecyl-2-oleoyl-*sn*-glycero-3-phosophocholine, PC(16:0e/18:1), ($[M + H]^+$), for m/z 746.5 was confirmed with LC−MS/MS (see the Supporting Information).

Lipid Imaging with C_{60}-SIMS. The SIMS spectrum, Figure 1, provides a rich array of molecules for imaging, see Figure 3.

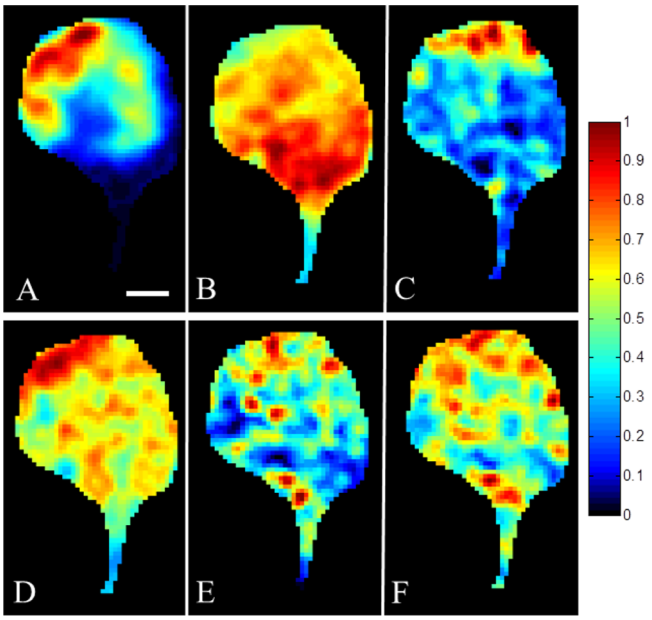

Figure 3. TOF-SIMS images obtained from a single *Aplysia* neuron: (A) vitamin E, α-tocopherol, $C_{29}H_{50}O_2$, $M^{\bullet}$, m/z 430.3, (B) hydrocarbon (m/z 128.1), (C) cholesterol, $C_{27}H_{45}$, $[M + H - OH]^+$ (m/z 369.3), (D) phosphocholine headgroup (m/z 184), $C_5H_{15}NPO_4$, $[M + H]^+$, (E) PC(16:0e/18:1) high-mass fragment (m/z 709.6), $C_{39}H_{75}O_7PNa$, $[M + Na - TMA]^+$, and (F) sum of PC(16:0e/18:1)-related peaks [m/z 709 ($C_{39}H_{75}O_7PNa$, $[M + Na - TMA]^+$), m/z 725 ($C_{39}H_{75}O_7PK$, $[M + K - TMA]^+$), m/z 746 ($C_{42}H_{85}NO_7P$, $[M + H]^+$), m/z 768 ($C_{42}H_{84}NO_7PNa$, $[M + Na]^+$), and m/z 784 ($C_{42}H_{84}NO_7PK$, $[M + K]^+$)]. (Scale bar = 100 μm.)

Some molecules can be detected intact (i.e., vitamin E and cholesterol; Figure 3, parts A and C); however, for some biomolecules sensitivity issues prevent the detection of intact species. In these cases, fragment ions are monitored instead (i.e., m/z 128 and m/z 184; Figure 3, parts B and D). The chemicals found on the surface of the cell provide information on the biochemistry of the cell; thus, the relative position of these molecules provides information on the possible function and chemical environment.

The protonated molecular ion of PC(16:0e/18:1) at m/z 746.6 was not observed at a high enough intensity to be imaged. However, the biological salt adducts at m/z 768.6 $[M + Na]^+$ and 784.6 $[M + K]^+$ were observed in the in situ SIMS spectrum along with their respective high-mass fragment ion at m/z 709.5 and m/z 725.5. The peak at m/z 709.5 had enough signal intensity to map its distribution across the neuron as

dx.doi.org/10.1021/ac303038j | *Anal. Chem.* XXXX, XXX, XXX−XXX

shown in Figure 3E. This ether lipid has a heterogeneous distribution within the soma. The higher relative intensity of PC(16:0e/18:1) in the upper portion of the soma is consistent with the mapped distribution of the phosphocholine headgroup at m/z 184. The summed contribution of the peaks related to the PC(16:0e/18:1) lipid (Figure 3F) improves the contrast of the image and improves the sensitivity of the technique.

Vitamin E Distribution. Vitamin E is a lipid which has been previously reported to be present on the surface of *Aplysia* neurons.[27,28] Monroe et al. found vitamin E localized to the junction of the cell soma and neurite, where it was believed to assist in the transportation of neurotransmitters and other important biomolecules from the location of synthesis (soma) to their release site (synapse).[27] In this report, the localization of vitamin E on the surface of the *Aplysia* neuron has a high correlation (83%) to the yellow-orange pigment, carotenoids,[37,38] observed in the optical image (see Figure 4C). It

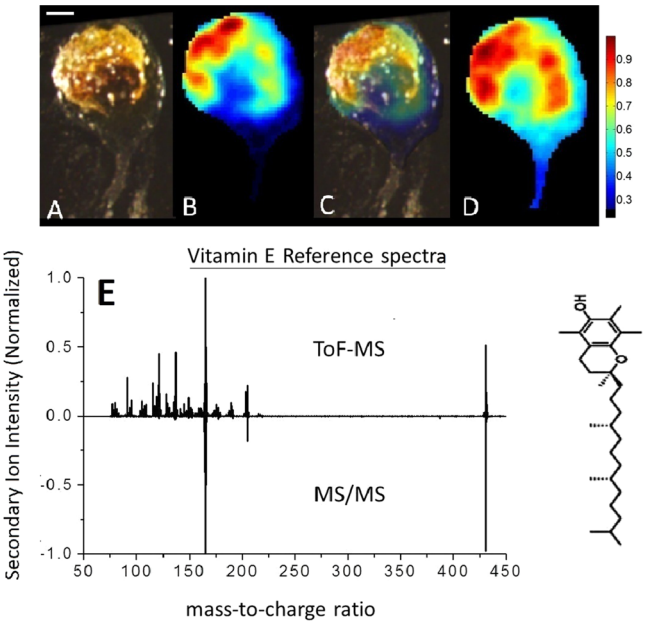

Figure 4. Optical image (A) and the TOF-SIMS image of vitamin E (B) was overlaid (C) to show the overlap of the vitamin E with the yellow-orange pigment. TOF-MS (panel E, top) and tandem MS of the protonated molecular ion at m/z 430.3 (panel E, bottom) reference spectra for vitamin E are shown. The tandem MS obtained from vitamin E reference material was used to extract and compile the vitamin E related peaks in the TOF-MS image of the *Aplysia* neuron in order to improve the sensitivity of the measurement (D). (Scale bar = 100 μm.)

is possible that vitamin E was original colocalized with the carotenoids but has migrated to the surface. Future, three-dimensional MS imaging of these cells in a frozen hydrated state may be beneficial to understanding the original location of the vitamin E. In addition, this report confirms the identification of vitamin E (α-tocopherol) with in situ tandem MS analyses.

TOF-MS and tandem MS reference spectra were obtained for vitamin E (α-tocopherol) using SIMS, Figure 4E. The main fragments in the vitamin E tandem MS reference spectrum are m/z 165.1 and 205.2, with minor contributions from the following peaks: m/z 90.9, 109, 120.9, 135.9, 146.1, 165, 177, and 191. These peaks are characteristic of the vitamin E gas-phase fragmentation pathway and are also prominent in the TOF-MS spectrum. The similarity between these two spectra suggests that gas-phase degradation after desorption may be a primary contributor to the fragmentation observed in SIMS-based spectra. An intensity-based correlation was performed in order to evaluate the similarities among these two spectra. The level of commonalities between two spectra was 0.75. Although this value shows a positive linear relationship between the two spectra it is not a particularly strong correlation.

The two reference spectra only have 61% of their peaks in common. One noticeable difference in these two reference spectra is the presence and high abundance of low-mass peaks in the TOF-MS spectrum. These peaks are not present in the tandem MS and may be the result of impurities, fragments produced by bombardment-related damage, postdesorption fragment degradation, or fragment interaction in the desorption plume.

Since the tandem MS reference spectrum provides the cleanest spectral representation of vitamin E, it has been used to compile the vitamin E related peak in the TOF-MS image obtained from the surface of a single *Aplysia* neuron. The dot product of the vitamin E tandem reference spectrum and the TOF-MS image data set was calculated using eq 1. In this equation, **X** represents the complex in situ TOF-MS data set for one pixel and **Y** represents the tandem MS reference spectrum.

$$\mathbf{X}\cdot\mathbf{Y} = \sum_{m/z=60}^{850} X_{m/z}Y_{m/z} = X_{60}Y_{60} + \ldots + X_{850}Y_{850} \quad (1)$$

The resulting image is shown in Figure 4D. This method is similar to principal component analysis (PCA), a data analysis method routinely used with TOF-SIMS data sets.[39−44] However, instead of correlating within the data set to find common trends, an external spectrum of the known compound is used. When the full data set is projected on the tandem MS reference spectra, the peaks that are characteristic of vitamin E are selected and compiled. This creates an image that is more descriptive of vitamin E and greatly improves the sensitivity of the technique.

Biological Significance. Vitamin E, an antioxidant, protects the brain from neuronal damage associated with oxidative stress. Its ability to reduce the risk or to slow down the progression of neurodegenerative diseases, such as Alzheimer's and Parkinson's disease, in clinical trials is controversial.[45−47] However, it is believed that vitamin E deficiency may alter neural communication via reducing signal conduction and contribute to neurological problems.[48]

In this investigation, the ether lipid PC(16:0e/18:1) has been identified as the dominant phospholipid species detected in the SIMS spectrum taken from the surface of a single *Aplysia* neuron. This lipid and other 1-*O*-alkyl-*sn*-glycero-3-phosphocholine lipids are known precursors to platelet-activating factor (PAF), an important cellular mediator involved with regulating inflammation.[49,50] PAF is multifunctional; it plays a role in immune response, blocks platelet aggregation, and stimulates enzymatic activity for various biological processes.[51,52] Currently, the role of PAF in neuronal function is not well-defined; however, it has been previously detected in the brain, suggesting a possible role in brain physiology.[52−55] Some sources have suggested that vitamin E enhances the acylation (i.e., deactivation) of PAF via indirectly stimulating the enzyme responsible for converting 2-lyso PAF(alkyl) into ether lipids (alkylacyl).[56−59] In one particular experiment, Tran et al. found

dx.doi.org/10.1021/ac303038j | Anal. Chem. XXXX, XXX, XXX−XXX

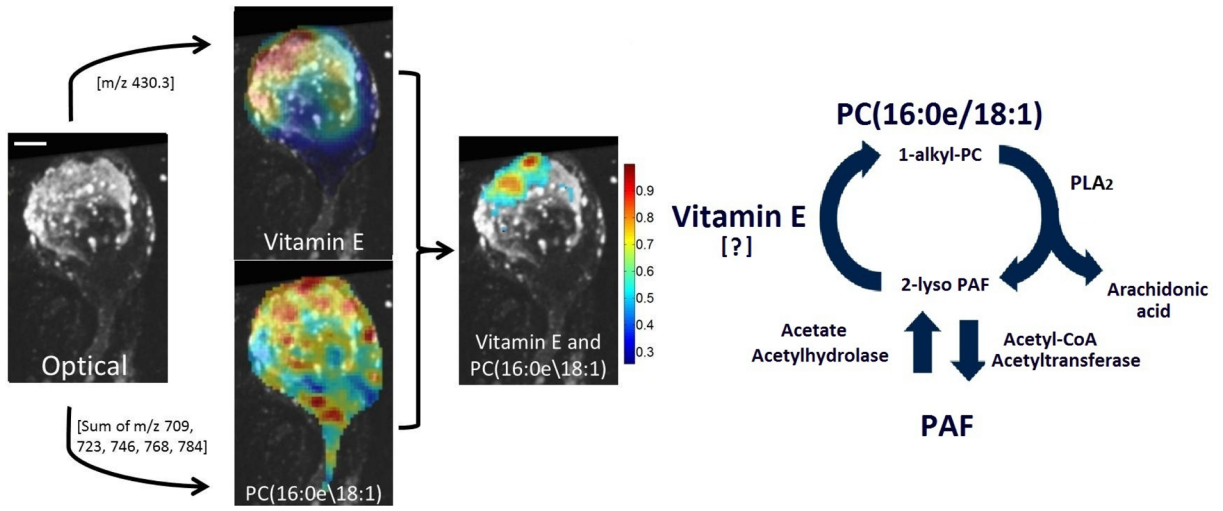

Figure 5. Vitamin E signal (m/z 430.3) and compiled PC(16:0e/18:1) lipid signal overlaid on the optical image. A region of high colocalization (threshold = 0.5) between the two chemicals can be seen in the upper portion of the soma. (Scale bar = 100 μm.)

an increased levels of ether lipids in cells incubated with vitamin E compared to control cells.[56]

With the high spatial resolution of C_{60}-SIMS, we have the ability to visualize the relative distributions of both the ether lipid PC(16:0e/18:1) and vitamin E on the surface of a single cell. A region of high colocalization between the vitamin E signal (m/z 430.3) and compiled PC(16:0e/18:1) lipid signal on the top portion of the neurons soma is illustrated in Figure 5. The ability to detect and elucidate the relative distribution of both these molecules on a single cell shows that the C_{60}-QSTAR is a potential platform for studying biochemical processes, such as innate immunity, when applied to macrophages. Since these cells are significantly smaller than the *Aplysia* cells present here, methods to improving the sensitivity of the system, such as tandem MS reference dot-product projections, are needed.

CONCLUSIONS

A multimodal approach was used to characterize lipids on the single-cell level. SIMS and tandem MS analyses were used to identify PC(16:0e/18:1) as the dominant lipid species observed on the surface of a single *Aplysia* neuron. Its partial localization with vitamin E, which is strongly localized with a visible cellular structure, may help to elucidate its role in cellular functions. The results presented here show that the C_{60}-QSTAR is a useful platform for studying lipids. On the single-cell level there is often a trade-off between sensitivity and lateral resolution. In this report, sensitivity is improved by compiling analyte peaks and their fragments, which are identified with tandem mass spectrometry. This model system provides a good starting point for future single-cell lipidomic investigations on mammalian cells, which are significantly smaller.

ASSOCIATED CONTENT

Supporting Information

Additional information as noted in text. This material is available free of charge via the Internet at http://pubs.acs.org.

AUTHOR INFORMATION

Corresponding Author

*E-mail: melissa.passarelli@gmail.com (M.K.P.); nxw@psu.edu (N.W.).

Notes

The authors declare no competing financial interest.

ACKNOWLEDGMENTS

The authors thank Professor Bob Murphy and Dr. Joseph Hankin for insight on lipid biochemistry and the LC−MS conformation analysis, Dr. Stanislav S. Rubakhin and Dr. Kevin Tucker from Professor Jonathan Sweedler' s group and Dr. Michael Heien for the preparation of the *Aplysia* samples, Dr. Alex Henderson for MATLAB data processing scripts, and Dr. Raphaël Trouillon for direction in the mathematical analyses. The authors acknowledge the LipidMAPS Consortium (GM069338-07) for financial support. Also additional financial support from the National Institutes of Health (2R01 EB002016-18) and the National Science Foundation (no. CHE-0908226) is appreciated.

REFERENCES

(1) Amstalden van Hove, E. R.; Smith, D. F.; Heeren, R. *J. Chromatogr., A* **2010**, *1217*, 3946−3954.
(2) Watrous, J. D.; Alexandrov, T.; Dorrestein, P. C. *J. Mass Spectrom.* **2011**, *46*, 209−222.
(3) Trouillon, R.; Passarelli, M. K.; Wang, J.; Kurczy, M.; Ewing, A. *Anal. Chem.* **2013**, *85*, 522−542.
(4) Colliver, T. L.; Brummel, C. L.; Pacholski, M. L.; Swanek, F. D.; Ewing, A. G.; Winograd, N. *Anal. Chem.* **1997**, *69*, 2225−2231.
(5) Lin, Y.; Trouillon, R.; Safina, G.; Ewing, A. G. *Anal. Chem.* **2011**, *83*, 4369−4392.
(6) Fletcher, J. S. *Analyst* **2009**, *134*, 2204−2215.
(7) Boggio, K. J.; Obasuyi, E.; Sugino, K.; Nelson, S. B.; Agar, N. Y. R.; Agar, J. N. *Expert Rev. Proteomics* **2011**, *8*, 591−604.
(8) Li, L.; Garden, R. W.; Sweedler, J. V. *Trends Biotechnol.* **2000**, *18*, 151−160.
(9) Ifa, D. R.; Wiseman, J. M.; Song, Q.; Cooks, R. G. *Int. J. Mass Spectrom.* **2007**, *259*, 8−15.
(10) Kleinfeld, A. M.; Kampf, J. P.; Lechene, C. *J. Am. Soc. Mass Spectrom.* **2004**, *15*, 1572−1580.
(11) Sun, S.; Szakal, C.; Smiley, E. J.; Postawa, Z.; Wucher, A.; Garrison, B. J.; Winograd, N. *Appl. Surf. Sci.* **2004**, *231*, 64−67.
(12) Winograd, N. *Anal. Chem.* **2005**, *77*, 142−149.
(13) Frazier, W. T.; Kandel, E. R.; Kupferma, I.; Waziri, R.; Coggesha, R. *J. Neurophysiol.* **1967**, *30*, 1288.
(14) Kandel, E. R.; Kriegstein, A.; Schacher, S. *Neuroscience* **1980**, *5*, 2033.

(15) Kriegstein, A. R. *Proc. Natl. Acad. Sci. U.S.A.* **1977**, *74*, 375.
(16) Kandel, E. R. *Science* **2001**, *294*, 1030.
(17) Halpern, J. M.; Xie, S.; Sutton, G. P.; Higashikubo, B. T.; Chestek, C. A.; Lu, H.; Chiel, H. J.; Martin, H. B. *Diamond Relat. Mater.* **2006**, *15*, 183−187.
(18) Marinesco, S.; Carew, T. J. *J. Neurosci.* **2002**, *22*, 2299−2312.
(19) Marinesco, S.; Carew, T. J. *J. Neurosci. Methods* **2002**, *117*, 87−97.
(20) Glanzman, D. L.; Mackey, S. L.; Hawkins, R. D.; Dyke, A. M.; Lloyd, P. E.; Kandel, E. R. *J. Neurosci.* **1989**, *9*, 4200−4213.
(21) Ciobanu, L.; Rubakhin, S. S.; Stuart, J. N.; Fuller, R. R.; Webb, A. G.; Sweedler, J. V. *Anal. Chem.* **2004**, *76*, 2331−2335.
(22) Kruse, R. A.; Rubakhin, S. S.; Romanova, E. V.; Bohn, P. W.; Sweedler, J. V. *J. Mass Spectrom.* **2001**, *36*, 1317−1322.
(23) Floyd, P. D.; Li, L.; Moroz, T. P.; Sweedler, J. V. *J. Chromatogr., A* **1999**, *830*, 105−113.
(24) Rubakhin, S. S.; Page, J. S.; Monroe, B. R.; Sweedler, J. V. *Electrophoresis* **2001**, *22*, 3752−3758.
(25) Garden, R. W.; Moroz, L. L.; Moroz, T. P.; Shippy, S. A.; Sweedler, J. V. *J. Mass Spectrom.* **1996**, *31*, 1126−1130.
(26) Zimmerman, T. A.; Rubakhin, S. S.; Sweedler, J. V. *J. Am. Soc. Mass Spectrom.* **2011**, 1−9.
(27) Monroe, E. B.; Jurchen, J. C.; Lee, J.; Rubakhin, S. S.; Sweedler, J. V. *J. Am. Chem. Soc.* **2005**, *127*, 12152−12153.
(28) Tucker, K. R.; Li, Z.; Rubakhin, S. S.; Sweedler, J. V. *J. Am. Soc. Mass Spectrom.* **2012**, 1−8.
(29) Piehowski, P. D.; Carado, A. J.; Kurczy, M. E.; Ostrowski, S. G.; Heien, M. L.; Winograd, N.; Ewing, A. *Anal. Chem.* **2008**, *80*, 8662.
(30) Hankin, J. A.; Barkley, R. M.; Murphy, R. C. *J. Am. Soc. Mass Spectrom.* **2007**, *18*, 1646−1652.
(31) Carado, A.; Passarelli, M. K.; Kozole, J.; Wingate, J. E.; Winograd, N.; Loboda, A. V. *Anal. Chem.* **2008**, *80*, 7921−7929.
(32) Benabdellah, F.; Seyer, A.; Quinton, L.; Touboul, D.; Brunelle, A.; Laprévote, O. *Anal. Bioanal. Chem.* **2010**, *396*, 151−162.
(33) Murphy, R. C.; Fiedler, J.; Hevko, J. *Chem. Rev.* **2001**, *101*, 479−526.
(34) Hsu, F. F.; Turk, J. *J. Am. Soc. Mass Spectrom.* **2003**, *14*, 352−363.
(35) Rebecca, W.; Sweedler, J. V. *Anal. Chem.* **2000**, *72*, 30−36.
(36) Passarelli, M. K.; Winograd, N. *Surf. Interface Anal.* **2011**, *43*, 269−271.
(37) Uéda, K.; Kawai, K. *Biochim. Biophys. Acta, Gen. Subj.* **1979**, *584*, 339−345.
(38) Petrunyaka, V. V. *Cell. Mol. Neurobiol.* **1982**, *2*, 11−20.
(39) Henderson, A.; Fletcher, J. S.; Vickerman, J. C. *Surf. Interface Anal.* **2009**, *41*, 666−674.
(40) Pacholski, M. L. *Appl. Surf. Sci.* **2004**, *231*, 235−239.
(41) Vaidyanathan, S.; Fletcher, J. S.; Henderson, A.; Lockyer, N. P.; Vickerman, J. C. *Appl. Surf. Sci.* **2008**, *255*, 1599−1602.
(42) Wagner, M. S.; Graham, D. J.; Ratner, B. D.; Castner, D. G. *Surf. Sci.* **2004**, *570*, 78−97.
(43) Graham, D. J.; Wagner, M. S.; Castner, D. G. *Appl. Surf. Sci.* **2006**, *252*, 6860−6868.
(44) Tyler, B. J.; Rayal, G.; Castner, D. G. *Biomaterials* **2007**, *28*, 2412−2423.
(45) Petersen, R. C.; Thomas, R. G.; Grundman, M.; Bennett, D.; Doody, R.; Ferris, S.; Galasko, D.; Jin, S.; Kaye, J.; Levey, A. *N. Engl. J. Med.* **2005**, *352*, 2379−2388.
(46) Dexter, D.; Jenner, P.; Ward, R. J.; Peter, T. J.; Wells, F. R.; Daniel, S. E.; Lees, A. J.; Marsden, C. D. *Ann. Neurol.* **1992**, *32*, 591−593.
(47) Etminan, M.; Gill, S. S.; Samii, A. *Lancet Neurol.* **2005**, *4*, 362−365.
(48) Gilgun-Sherki, Y.; Melamed, E.; Offen, D. *Neuropharmacology* **2001**, *40*, 959−975.
(49) Lenihan, D. J.; Lee, T. C. *Biochem. Biophys. Res. Commun.* **1984**, *120*, 834−839.
(50) Snyder, F. *Biochem. J.* **1995**, *305*, 689.
(51) Demopoulos, C. A.; Pinckard, R. N.; Hanahan, D. J. *J. Biol. Chem.* **1979**, *254*, 9355−9358.
(52) Shimizu, T.; Honda, Z.; Nakamura, M.; Bito, H.; Izumi, T. *Biochem. Pharmacol.* **1992**, *44*, 1001.
(53) Bito, H.; Nakamura, M.; Honda, Z.; Izumi, T.; Iwatsubo, T.; Seyama, Y.; Ogura, A.; Kudo, Y.; Shimizu, T. *Neuron* **1992**, *9*, 285−294.
(54) Kumar, R.; Harvey, S. A. K.; Kester, M.; Hanahan, D. J.; Olson, M. S. *Biochim. Biophys. Acta, Lipids Lipid Metab.* **1988**, *963*, 375−383.
(55) Hattori, M.; Adachi, H.; Tsujimoto, M.; Arai, H.; Inoue, K. *Nature* **1994**, *370*, 216−218.
(56) Tran, K.; D'Angelo, A. F.; Choy, P. C.; Chan, A. C. *Biochem. J.* **1994**, *298*, 115.
(57) Fukuzawa, K.; Kurotori, Y.; Tokumura, A.; Tsukatani, H. *Ann. N.Y. Acad. Sci.* **1989**, *570*, 449−454.
(58) Fukuzawa, K.; Kurotori, Y.; Tokumura, A.; Tsukatani, H. *Lipids* **1989**, *24*, 236−239.
(59) Kakishita, E.; Suehiro, A.; Oura, Y.; Nagai, K. *Thromb. Res.* **1990**, *60*, 489−499.